JOURNAL OF GEOPHYSICAL RESEARCH, VOL. 115, E06008, doi:10.1029/2009JE003491, 2010

Detection of small lunar secondary craters in circular polarization ratio radar images

Kassandra S. Wells,[1] Donald B. Campbell,[1] Bruce A. Campbell,[2] and Lynn M. Carter[2]

Received 20 August 2009; revised 4 February 2010; accepted 22 February 2010; published 17 June 2010.

[1] The identification of small (D < a few kilometers) secondary craters and their global distributions are of critical importance to improving our knowledge of surface ages in the solar system. We investigate a technique by which small, distal secondary craters can be discerned from the surrounding primary population of equivalent size based on asymmetries in their ejecta blankets. The asymmetric ejecta blankets are visible in radar circular polarization ratio (CPR) but not as optical albedo features. Measurements with our new technique reveal 94 secondary craters on the Newton and Newton-A crater floors near the lunar south pole. These regions are not in an obvious optical ray, but the orientation of asymmetric secondary ejecta blankets suggests that they represent an extension of the Tycho crater ray that crosses Clavius crater. Including the secondary craters at Newton and Newton-A skews the terrain age inferred by crater counts. It is reduced by few percentages by their removal, from 3.8 to 3.75 Gyr at Newton-A. Because "hidden rays" like that identified here may also occur beyond the edges of other optically bright lunar crater rays, we assess the effect that similar but hypothetical populations would have on lunar terrains of various ages. The average secondary crater density measured at 1 km diameter is equivalent to the crater density at 1 km on a 3.4 Gyr surface [*Neukum et al.*, 2001]. Younger surfaces (i.e., younger crater ejecta blankets) would be dominated by secondary craters below 1 km if superposed by a hidden ray.

Citation: Wells, K. S., D. B. Campbell, B. A. Campbell, and L. M. Carter (2010), Detection of small lunar secondary craters in circular polarization ratio radar images, *J. Geophys. Res.*, *115*, E06008, doi:10.1029/2009JE003491.

1. Introduction

[2] In his preliminary work studying lunar crater distributions, Shoemaker identified two populations of craters with differing power law cumulative frequency slopes. The shallower branch he labeled "primary" and attributed to impacts from interplanetary bolides, whereas the steeper "secondary" branch he theorized could be the footprints of ejecta from large primary impacts [*Shoemaker*, 1965]. Since this early work, crater counting and classification has become increasingly important in the context of providing ages for surfaces on solid planets, and Shoemaker's original arguments concerning the relative dominance of secondary and primary craters in the steep branch have come under scrutiny. Some workers [*McEwen et al.*, 2005; *Bierhaus et al.*, 2001, 2005; *Hurst et al.*, 2004] claim that secondaries form a significant contaminant of crater counts used for age dating, while others suggest that the contamination from secondary impacts on Martian surfaces, for instance, may be minimal (~10% of craters with D < 1 km [*Werner et al.*, 2009]) and argue that the secondary branch does not arise from ejecta fallback from primaries at all but from a smaller class of interplanetary bolides [*Neukum and Wise*, 1976; *Neukum*, 1983; *Neukum and Ivanov*, 1994].

[3] Some of the controversy surrounding the issue stems from the difficulty of discerning small primaries from distal secondaries [*McEwen et al.*, 2005; *Bierhaus et al.*, 2005]. Near the parent primary, secondary impact craters form with low velocities and are identified by their unique morphologies (high ellipticities, shallow profiles, tendency to form in clusters, and the occasional presence of "herringbone" or chevron-shaped ridges that usually point down trajectory from the primary [*McEwen et al.*, 2005; *Pike and Wilhelms*, 1978; *Oberbeck and Morrison*, 1973]).

[4] Because of the increase in velocity with distance from the impact, the resulting distal secondary crater morphologies are more reminiscent of primary impacts than their proximal counterparts. They tend to be more circular and lack the characteristically flat, shallow floors of near-field secondaries [*McEwen et al.*, 2005]. Also, given the higher ejecta velocities, there is a greater chance that distal ejecta fragments will spread in the transverse direction, possibly reducing the clustering that aids in identification of secondaries at closer ranges [*Bierhaus et al.*, 2005]. Despite these difficulties, it is important to devise a method for identifying these distant secondaries and their origins, as size frequency distributions (SFDs) of small craters (D < a few kilometers) must be well constrained in order to accu-

[1] Astronomy and Space Sciences Department, Cornell University, Ithaca, New York, USA.
[2] Center for Earth and Planetary Studies, National Air and Space Museum, Smithsonian Institution, Washington, District of Columbia, USA.

0148-0227/10/2009JE003491

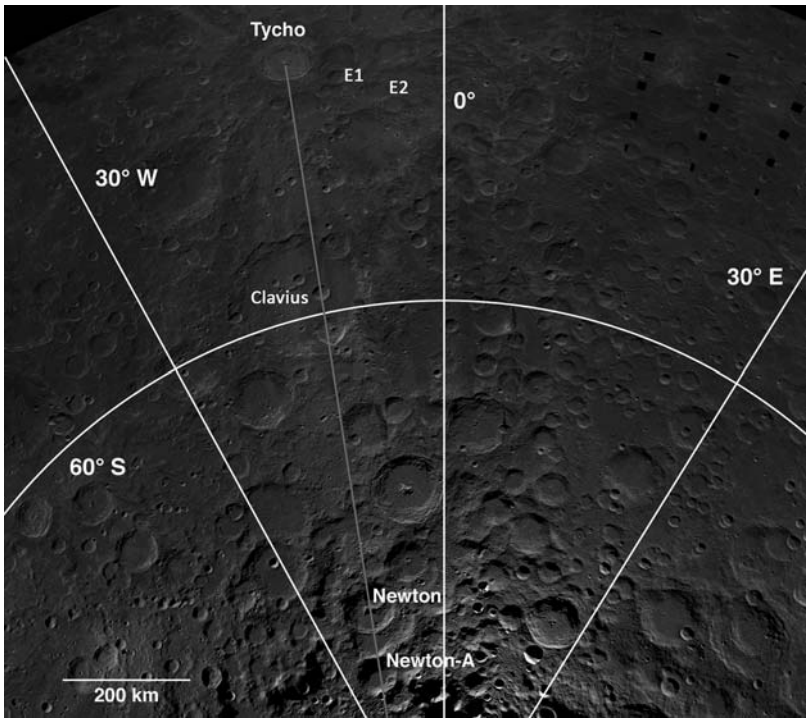

Figure 1. The Tycho crater ray (red line) extending south and crossing Newton and Newton-A craters as seen in a Clementine 750 nm image of the lunar south pole. Secondary craters identified in this work were found on the floors of these craters with ejecta blankets parallel to the highlighted Tycho ray. Image courtesy of the LPI Clementine mapping project.

rately date young terrains [*McEwen et al.*, 2005; *Bierhaus et al.*, 2001].

[5] In this vein, we present 20 m resolution single-channel (same sense of circular polarization as transmitted) and 100 m resolution circular polarization ratio (CPR), 13 cm radar data of the floors of lunar craters Newton (D = 79 km; 76.7°S, 16.9°W) and Newton-A (D = 64 km; 79.7°S, 19.7°W). These regions are not within an optical ray but just beyond a prominent Tycho ray stretching across Clavius crater (Figure 1). However, many small craters on the floors of Newton and Newton-A display distinctive ejecta blankets with prominent asymmetry down trajectory from Tycho crater (D = 85 km; 43.3°S, 11.2°W) (Figure 2), suggesting they are secondary craters belonging to that primary. The density of these secondary craters, as well as the orientation of their ejecta blankets, is consistent with the optical ray and may represent a "hidden" extension of that structure. We note that this area may have previously been optically bright and weathered to its present condition. For a discussion of the evolution and origin of lunar rays, see *Hawke et al.* [2004]. We explore the implications of this and other hypothetical "hidden ray" secondary crater populations on lunar age dating from small crater counts.

2. Data Set

[6] The images of the lunar south pole used in this work were acquired on 15 September 2006 by transmitting a single sense of circularly polarized, 2.38 GHz (13 cm) radiation from Arecibo Observatory and receiving the reflected lunar echo in both senses at the Green Bank Telescope (GBT) in Green Bank, WV [*Campbell et al.*, 2006]. The CPR maps represent the ratio of same sense (as transmitted; SC for "same circular") of received polarization to opposite sense (OC for "opposite circular") and can be used to deduce wavelength-scale roughness properties of the reflecting surface. A specular reflecting surface gives a CPR of 0 because the sense of circular polarization is reversed upon reflection, while more same-sense radiation is returned due to diffuse scattering. The classification of secondary craters discussed here hinges on this property; the secondary craters have asymmetric ejecta blankets, which show up in the CPR because they are rough and blocky on spatial scales comparable to the radar wavelength. There is greater contrast between these ejecta blankets and the background on smooth surfaces (i.e., when the background CPR is low). As a result, this technique is best suited for investigation of secondary craters in the maria or other smooth regions. A prevalence of these elongated ejecta blankets occurs on the floors of Newton, Newton-G, and Newton-A craters near the lunar south pole (Figure 2). At a distance of greater than 1000 km, the secondary craters visible in the CPR image at Newton and Newton-A are some of the furthest secondary craters from the Tycho impact examined to date. Similar distal Tycho secondary craters were identified in Ranger 7 spacecraft images of Mare Cognitum, also at a radial distance of about 1000 km [*Wilhelms et al.*, 1978]. *Dundas and McEwen* [2007] also investigated the density of distal Tycho craters in rays in Mare Cognitum and near Ptolemaeus crater (~1100 km from Tycho, similar to the distance between Tycho and Newton-A) and estimated based on their counts that Tycho produced at least 10^6 secondary craters with

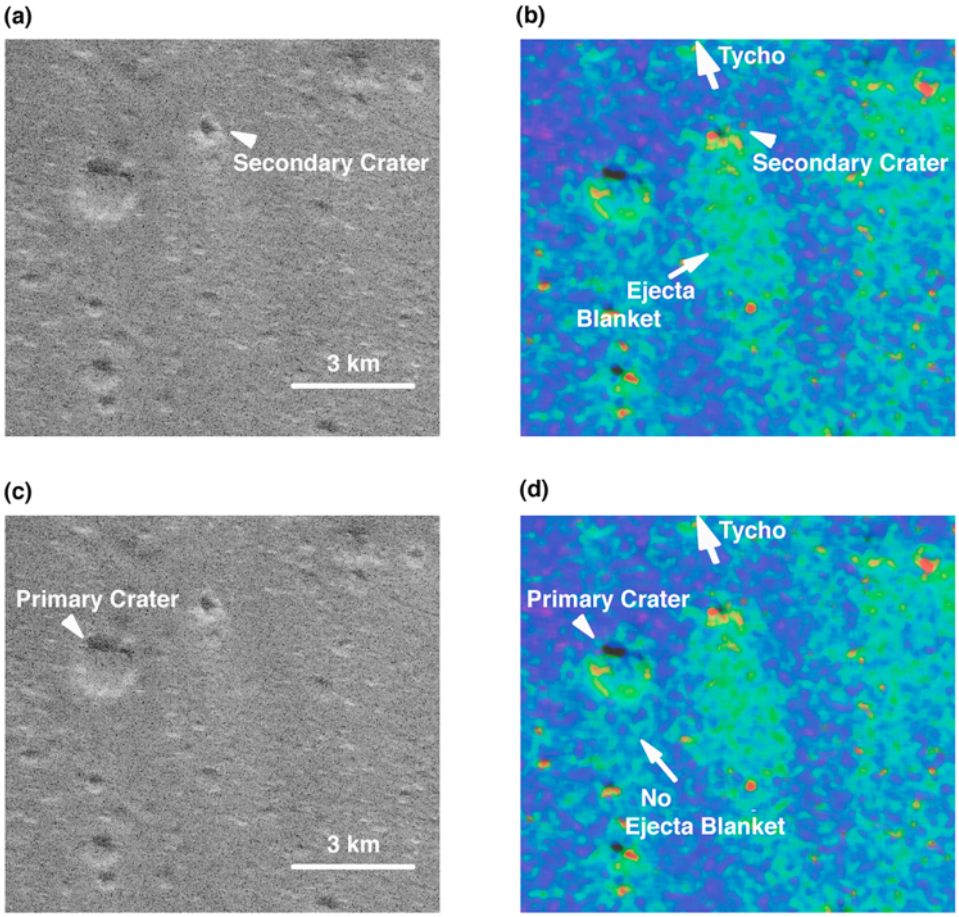

Figure 2. (a) A secondary crater in the SC radar channel image. (b) The same secondary crater in the CPR image. The ejecta blanket of the secondary crater, in comparison to that of the primary crater, is absent in the direction facing Tycho but elongated down trajectory. (c) A typical primary crater in the SC radar channel image. (d) The same primary crater in the CPR image. Note that the ejecta blanket, while visible in the CPR, is highly symmetric.

diameters greater than 63 m. However, they stress that this is a lower bound on secondary crater production that does not include secondary craters between or beyond rays evident in albedo or compositional maps. Work on Mars [*McEwen et al.*, 2005; *Preblich*, 2005] and Europa [*Bierhaus et al.*, 2001] suggests that these populations external to obvious rays may dominate the secondary crater production of a given event. An order of magnitude of more secondary craters belonging to the small, rayed Martian crater Zunil lies between obvious rays than in them, out to distances of 700 km. Three times more secondary craters are still beyond these rays entirely (distances > 700 km) [*Preblich*, 2005]. The secondary craters identified in this work are not encompassed by the 560,000 km^2 of Tycho rays identified by *Dundas and McEwen* [2007] and, therefore, probe this important parameter space for secondary cratering for the first time on the Moon.

3. Method

3.1. Primary Versus Secondary Crater Classification

[7] Because of the sensitivity of cratering statistics to the counting method employed, much care was taken to ensure that both crater counting and primary/secondary classification were as systematic as possible. Crater diameters were measured by fitting ellipses to crater rims. According to convention, the minor axes of the fitted ellipses were used for the crater diameters, but the major axis size and thus crater eccentricity were also recorded. The regions in which craters with 400 m $\leq D \leq$ 2 km were counted were an area of 3644 km^2 on the floors of Newton and Newton-G craters (henceforth: Newton region) and another of 996 km^2 on the floor of Newton-A crater (henceforth: Newton-A region).

[8] A major contribution to the uncertainty of secondary classification was the difficulty in establishing one-to-one correspondence between small craters and unresolved secondary ejecta blankets. A particular challenge was in distinguishing which of the craters in the ejecta blankets were responsible for the ejecta and which had merely been superposed by it. To help break the degeneracy, the simultaneous age of the Tycho secondary craters was employed. Because of the shared age of Tycho and its secondary craters and the assumed homogeneity of the lunar terrain in the relatively small regions of interest, the rim morphology of all Tycho secondary craters in the study should be equally degraded. Tycho crater is an extremely young (96 ± 5 Myr

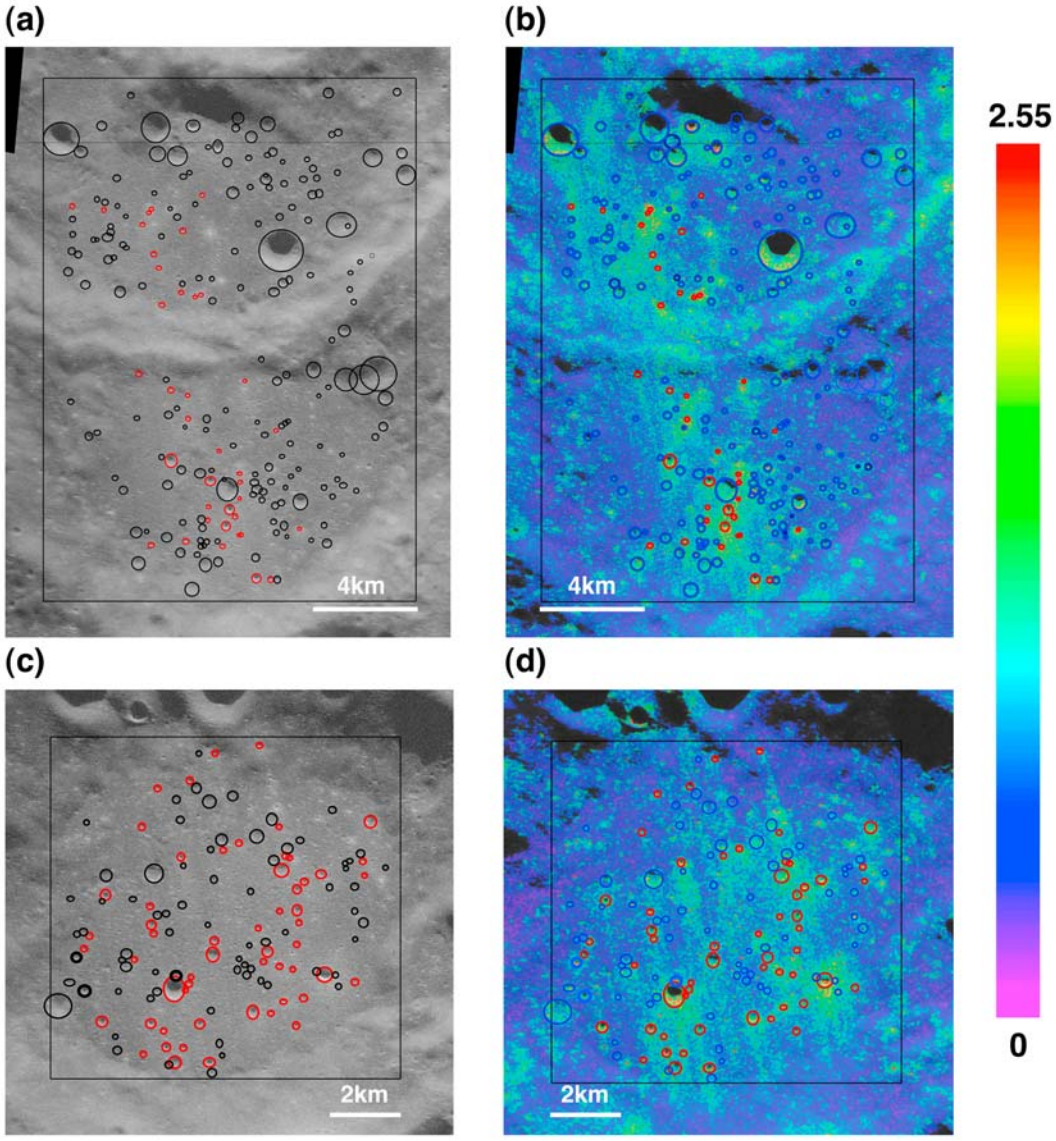

Figure 3. All craters counted in the Newton (Figures 3a and 3b) and Newton-A (Figures 3c and 3d) regions. Primary craters are marked in black/blue; secondary craters are in red. (a) 20 m/pixel single-channel image of Newton and Newton-G craters. (b) The Newton region in 100 m/pixel CPR. (c) The single-channel, 20 m/pixel image of the Newton-A region used for counting craters. (d) The Newton-A region in the CPR.

[*Arvidson et al.*, 1976]) lunar crater, and its secondary craters should be among the freshest-looking small-impact features in the Newton and Newton-A regions. According to the work of *Neukum et al.*'s [2001] lunar isochrons, on the order of only a few craters younger than 100 Myr with 400 m $\leq D \leq$ 2 km are expected in areas the size of Newton and Newton-A.

[9] Therefore, we can distinguish between Tycho secondaries and underlying primaries in the unresolved secondary ejecta blankets based on the crater rim morphology. A threefold classification system for rim freshness (in the single-channel image) was devised for this purpose: S for the craters with the sharpest rims, SD for craters with moderate rim degradation, and D for craters with diffuse, heavily degraded rims. All craters with classifications S and SD in unresolved secondary ejecta blankets as well as all craters with resolved secondary ejecta blankets were classified as secondary craters. Primary craters were those classified as D craters in regions of unresolved secondary ejecta blankets, all craters with no obviously correlated secondary ejecta blanket, and S and SD craters with symmetric or no ejecta blankets. We note that use of this type of morphological classification to correlate individual craters to asymmetric ejecta blankets is somewhat subjective, but the reader is reminded that secondary craters are typically identified on the basis of differences in morphology. In total, 445 craters were counted in the two regions, 94 of which were classified as secondary craters (Figure 3).

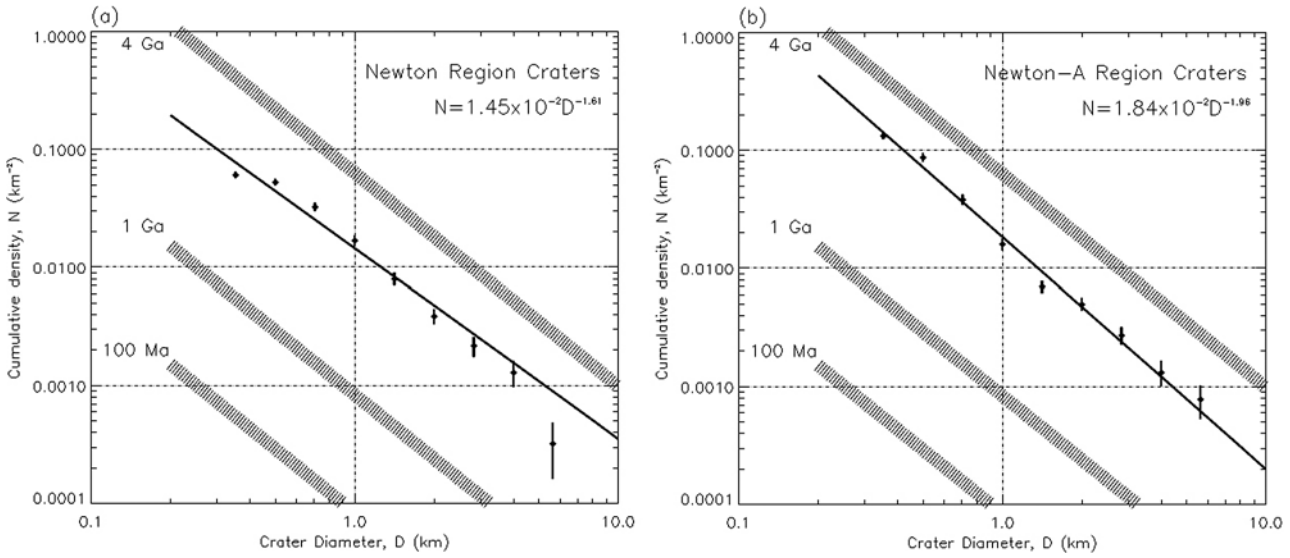

Figure 4. The cumulative size frequency distribution of all craters counted in (a) the Newton region and (b) the Newton-A region. The isochrons in Figures 1–9 follow *Neukum et al.* [2001].

3.2. Size Frequency Distributions

[10] The size frequency distributions of craters were compiled according to the recommendations set forth by the *Crater Analysis Techniques Working Group* [1979]. In addition to the craters already counted with 400 m < D < 2 km, all craters with diameters greater than 2 km were counted in larger regions including but also extending beyond the floors of Newton and Newton-A (12,442 km^2 at Newton and 12,877 km^2 at Newton-A). This was done in order to reduce small number statistics for the larger craters. The resulting cumulative and relative size frequency plots take the varying areas into account and are binned with $\sqrt{2}$ or $\sqrt{2}/2$ widths centered on 1 km. The first type of SFD compiled was the cumulative density plot, in which the number density of craters greater than a given diameter is plotted against the crater diameter (Figures 4, 5, and 6). Crater SFDs are power law functions of the form:

$$N(\geq D) = cD^{-b}, \tag{1}$$

where c and b are constants and D is the crater diameter. In log-log space, b is the slope of the distribution. In addition to the cumulative plots, differential or "R plots" were also generated for the data (Figure 7).

[11] The error bars for our crater counts represent the Poisson statistical counting noise associated with the total number of counts in each diameter bin. In order to assess the completeness of our counts in more than just the statistical sense, we compare the total number of secondary craters

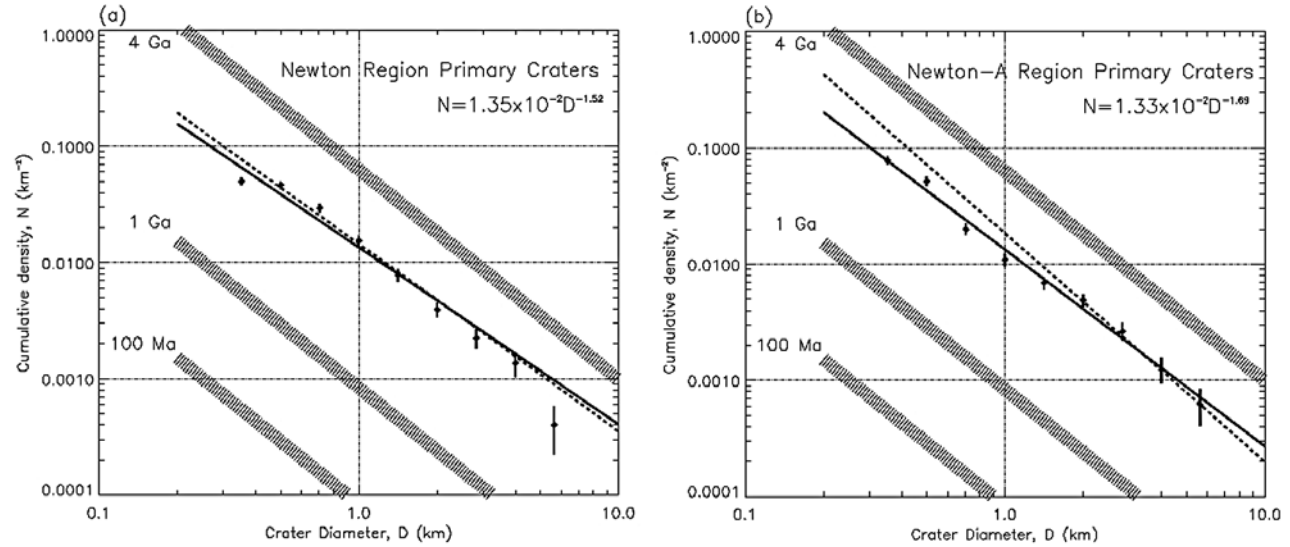

Figure 5. The cumulative size frequency distribution of the corrected primary craters (after removal of secondary craters) in (a) the Newton region and (b) the Newton-A region. The dotted line represents the fit to the crater distribution calculated before the removal of the secondary craters.

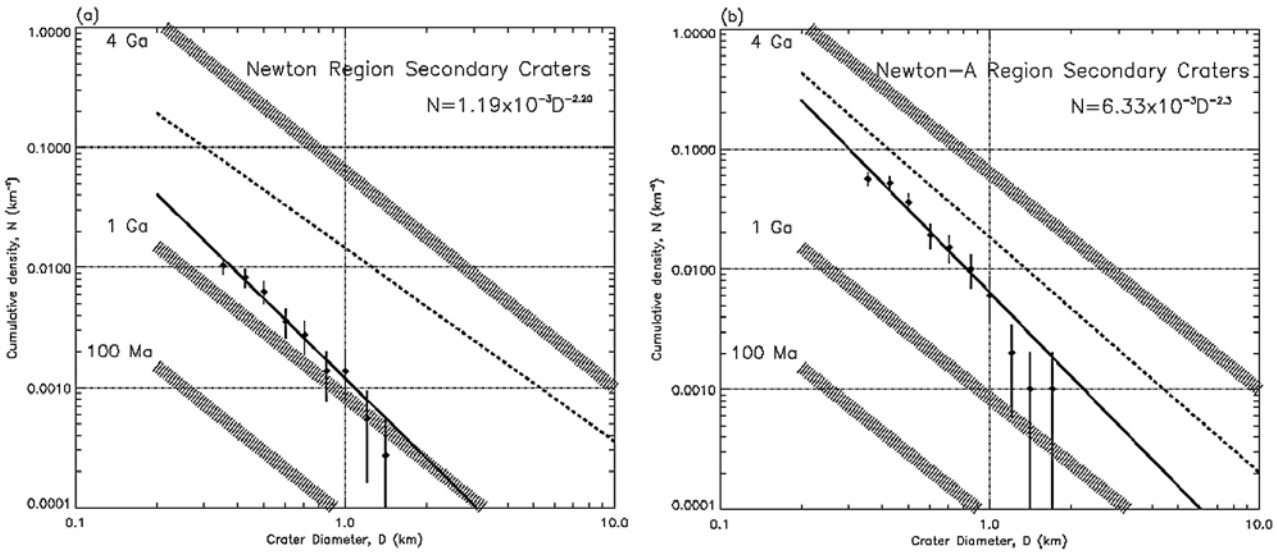

Figure 6. Cumulative size frequency distributions of the secondary craters identified at the (a) Newton region and (b) Newton-A region. The dotted line represents the combined distribution of primary and secondary craters first counted in the areas.

identified by *Hirata and Nakamura* [2006] in two regions to the east of Tycho, designated "E1" and "E2," to counts obtained with our method in those same areas (Figure 1). The results of this comparison are displayed in Table 1. In these regions, it appears that the radar method is less sensitive to counts of small craters than the optical method. The reason for this is probably twofold. First, the radar return is sensitive to the surface roughness, and region E1, in particular, has a very high background roughness because of its proximity to Tycho crater's continuous ejecta blanket. Therefore, it is more difficult to make out small crater rims against the background. Second, the radar incidence angle is relatively low at the latitude of Tycho crater, reducing radar shadow that also aids in the recognition of small craters. These two factors are less important on the relatively smooth floors of Newton and Newton-A craters, where the radar incidence angle is also very high (near grazing) due to the near-polar latitude. In any case, these viewing properties should affect the counting of secondary and primary craters roughly equally.

4. Results

4.1. Secondary Crater Populations and Comparison to Other Work

[12] Lunar primary craters exhibit a $b = -1.8$ slope in a cumulative size frequency distribution as compared to the steeper, $b = -3$ or -4 slope seen at crater diameters of less than a few kilometers. The interpretation that this steep branch is composed of secondary impacts was suggested by

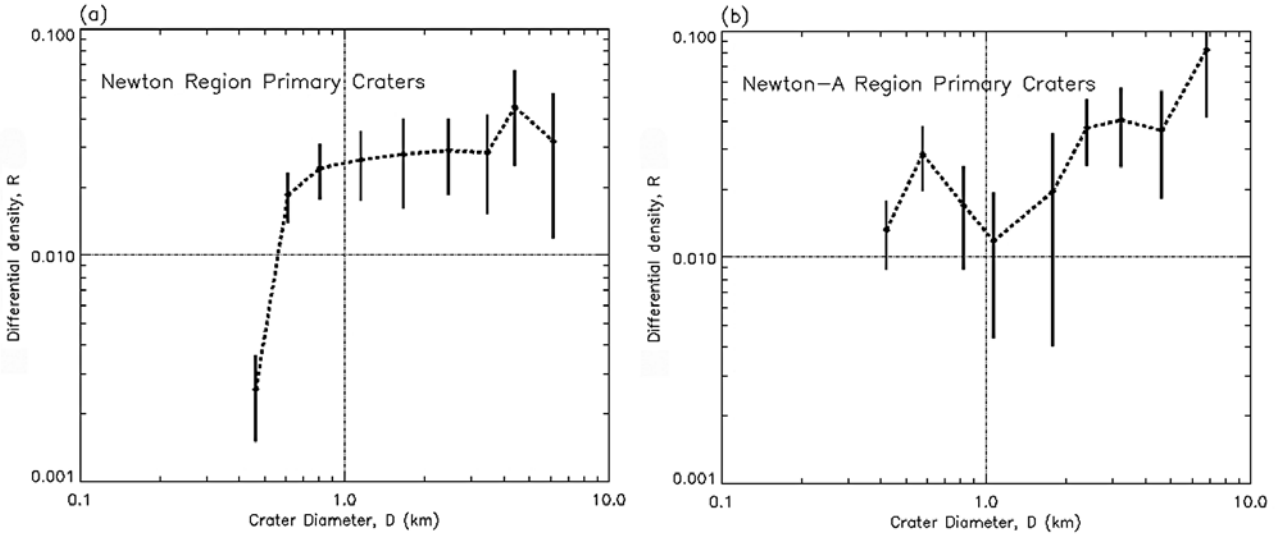

Figure 7. A differential plot (R plot) of the corrected primary crater populations at the (a) Newton region and (b) Newton-A region. Note the lack of craters counted in the 1 km and 1.717 km bins at Newton-A.

Table 1. A Comparison Between the Number of Secondary Craters[a]

	Tycho Distance (km)	Counting Area (km^2)	Number of Secondary Craters[b]	Number of Secondary Craters[c]	Cutoff Diameter for Power Law Fit[b]	Power Law Fit[b]
E1	130	1344	92 (35)[d]	98	1.7 km	$N(\geq D) = (1.32 \pm 0.11) \times 10^{-1} D^{-3.44 \pm 0.11}$
E2	190	4404	145 (52)[d]	55	1.0 km	$N(\geq D) = (1.26 \pm 0.07) \times 10^{-2} D^{-3.82 \pm 0.15}$

[a]Identified near Tycho crater by *Hirata and Nakamura* [2006] and the radar CPR method employed here. The cutoff diameter is relevant only to the power law fits of *Hirata and Nakamura* [2006] (i.e., not to the total counts). The necessity of a cutoff for fitting illustrates that secondary crater populations tend to "turn down" from their characteristic steep power law slopes in this size range.
[b]*Hirata and Nakamura* [2006].
[c]CPR and tertiary ejecta blanket method.
[d]Number of craters used for best fit calculation.

Shoemaker [1965] and has been more recently discussed in the works of *Hirata and Nakamura* [2006] and *Dundas and McEwen* [2007].

[13] In their analysis, *Hirata and Nakamura* [2006] found 92, 145, 134, and 98 secondary craters in regions at distances of 130, 190, 250, and 370 km from the Tycho primary, respectively. The cumulative SFDs of these four regions displayed characteristic power law slopes ranging between $b = -3.32$ and $b = -3.82$. The secondary craters surveyed by *Hirata and Nakamura* [2006] range in size from 0.55 km $< D <$ 4.0 km as compared to the Newton and Newton-A regions, where the largest secondary craters observed had diameters just under 2 km. The secondary crater densities measured by *Hirata and Nakamura* [2006] suggest that crater density does not decrease at a constant rate with distance from the primary but rather levels off after a few crater radii. The secondary craters at Newton and Newton-A fit this trend. The secondary densities at Newton-A (1108 km from Tycho), $c = 6.33 \times 10^{-3}$ craters/km^2, and at Newton (1015 km from Tycho), $c = 1.19 \times 10^{-3}$ craters/km^2, are only slightly lower than the 6.81×10^{-3} craters/km^2 measured by *Hirata and Nakamura* [2006] at 370 km from Tycho.

[14] The shallow power law slopes of $b = -2.20$ at Newton and $b = -2.30$ at Newton-A are seemingly unusual for secondary crater populations, which are often characterized by their steep power law forms. However, there is a well-documented, prominent downturn (i.e., a shallow power law slope) in the cumulative SFD of secondary craters that commonly occurs near diameters of about a kilometer, seemingly independent of distance from the primary crater [*Hirata and Nakamura*, 2006; *Arvidson et al.*, 1976; *Wilhelms et al.*, 1978]. The shallow power law slopes at Newton and Newton-A support this claim [*Arvidson et al.*, 1976; *Wilhelms et al.*, 1978]. When larger secondary craters are available, small craters in the regime of the downturn are not typically included for power law fitting. *Hirata and Nakamura* [2006] derived steep power law slopes for secondary craters above this downturn; for smaller craters, the slopes are similar to those seen in the small diameter population sampled at Newton and Newton-A. *Hirata and Nakamura* [2006] attribute the downturn to the destruction of small craters by the surges of ejecta generated by the many simultaneous impacts involved in the formation of a field of secondary craters. *Dundas and McEwen* [2007] also see shallow slopes within Tycho rays near Ptolemaeus crater but do not explicitly state the power law slopes for these distributions. They suggest that, generically, such downturns in the secondary crater SFD in rayed areas could be attributed to a number of factors, ranging from surges during emplacement that obliterate underlying or smaller craters, differential erasure of craters after emplacement due to surrounding slopes, observational incompleteness near the edge of resolution, and possibly the "true rollover" diameter at which ejecta production from primary craters deviates from the typical steep power law. However, this diameter is not well constrained, and higher-resolution images are needed to distinguish between these factors at Newton and Newton-A.

4.2. Primary Crater Populations

[15] The cumulative SFDs for the corrected (i.e., after the removal of the secondary craters) crater populations with 400 m $\leq D \leq$ 8 km are shown in Figure 5. Much like the downturn at small diameters in the secondary crater population, we expect that the primary cumulative SFD will level off due to saturation equilibrium. While the Newton region primary craters exhibit a plateau in the cumulative distribution at $D \leq$ 500 m, the Newton-A primary craters do not. Instead, there is a slight apparent excess of primary craters at these diameters. To clarify the issue, consider the differential R plot size frequency distribution (Figure 7).

[16] Because each bin stands alone, the differential SFD not only illuminates intrinsic differences in the crater population over various diameters but also reveals the unequal distribution of counting error throughout the sample. The R plot shows that the kink present in the cumulative plot may be attributed to the effects of small number statistics on the midrange bins with 1.717 km $\leq D <$ 2 km. This bin shows an anomalously low density with respect to the other size ranges, a property that translates to a temporary leveling off of the cumulative SFD in this region. The expected number of small primaries (for a $b = -1.8$ SFD) produces an artificially steepened branch in comparison to this momentary "plateau" in the cumulative distribution. The relative dearth of primary craters recorded in this bin is thus simply an artifact of the limited area available for study in the Newton and Newton-A crater floors. This case study illustrates an important point about the difficulties in interpreting cratering statistics for units of small spatial extent.

5. Discussion

5.1. Crater Count Contamination

[17] An important part of the controversy surrounding secondary impact craters is the effect of secondary cratering on the inferred ages of young surfaces. Terrains in obvious ray systems are not age-dated using crater counts because of

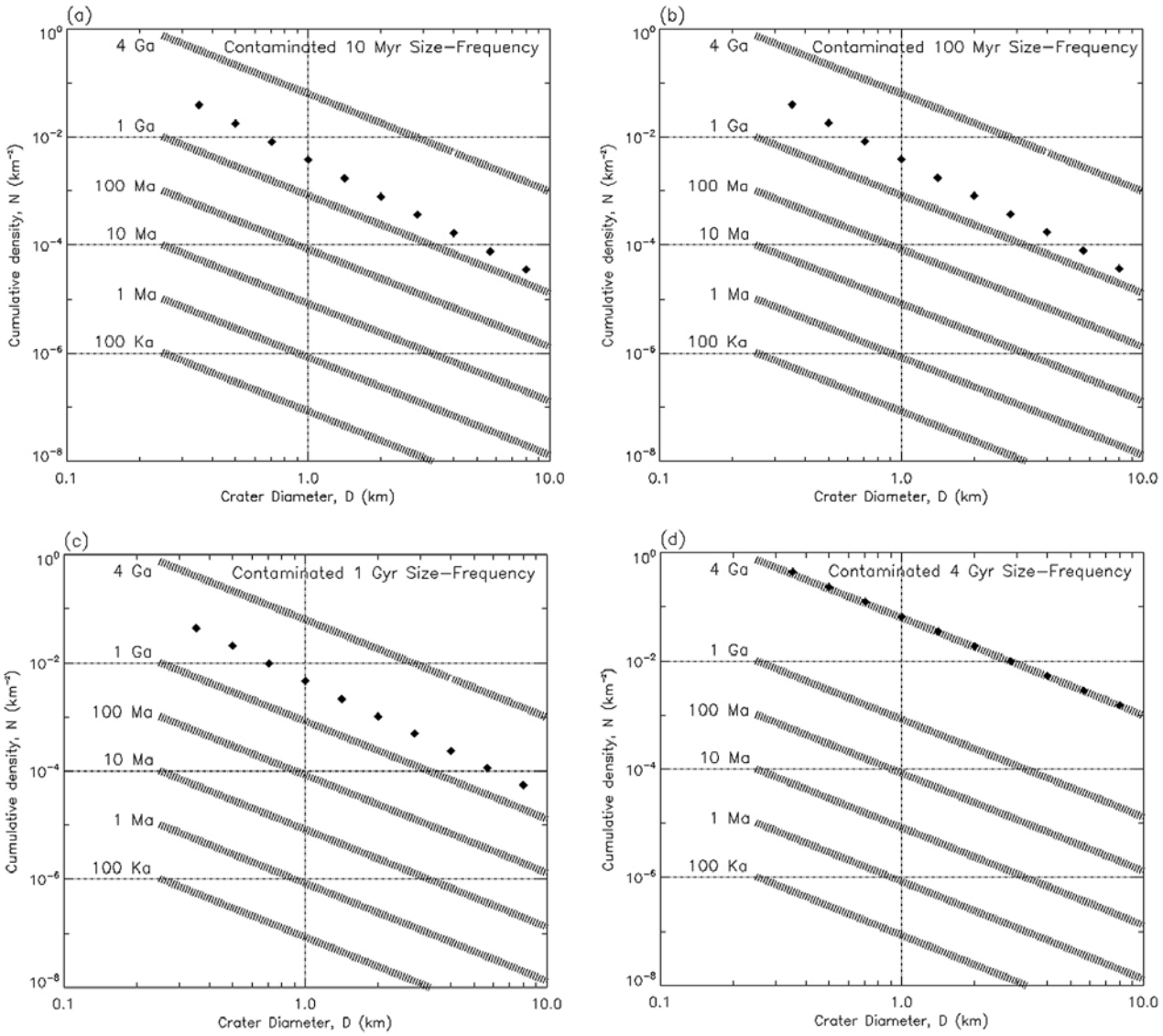

Figure 8. A secondary crater population similar to those measured here, with $N(\geq D) = 3.8 \times 10^{-3} \times D^{-2.25}$, emplaced on hypothetical lunar terrains with cumulative size frequency distributions as given by *Neukum et al.* [2001]. Specifically, secondary contamination of (a) 10 Myr old lunar terrain, (b) 100 Myr old lunar terrain, (c) 1 Gyr old lunar terrain, and (d) 4 Gyr old terrain. The shaded lines correspond to the ideal cases; diamonds represent populations contaminated by secondary craters.

the obvious contamination by secondary craters. However, our measurements suggest that the floors of Newton and Newton-A may belong to a "hidden" extension of a known Tycho ray. Because this portion of the ray is only apparent in the radar CPR, it could be mistaken as "ray-free" terrain and included in crater counts by workers relying only on optical images. Therefore, we compare the incorrect age that would be determined from such a count with the more accurate age determined after the removal of the secondary craters associated with the "hidden" ray.

[18] Including the secondary craters, the best fit power law inferred for Newton-A was $N(\geq D) = (1.84 \pm 0.07) \times 10^{-2} D^{(-1.96 \pm 0.05)}$ and $N(\geq D) = (1.45 \pm 0.06) \times 10^{-2} D^{(-1.61 \pm 0.05)}$ for Newton. Using *Neukum et al.*'s [2001] lunar isochrons, these distributions correspond to ages of 3.80 and 3.76 ± 0.01 Gyr, respectively. After removal of the identified Tycho secondary craters, the density constant measured for Newton-A region was $c = (1.33 \pm 0.06) \times 10^{-2}$ and $c = (1.35 \pm 0.05) \times 10^{-2}$ for Newton. These coefficients correspond to ages similar to those of the uncorrected population, at about 3.75 Gyr for Newton and Newton-A (Figure 5). The age inferred from the corrected primary counts suggests that resurfacing by impact melt from nearby Orientale basin (~3.8 Gyr) may be responsible for the relatively smooth Newton and Newton-A craters floors [*Wilhelms et al.*, 1979; *Campbell and Campbell*, 2006].

[19] It is possible that other such "hidden rays" exist on the lunar surface. Assuming that Newton and Newton-A are representative samples, "hidden" secondary crater populations have the potential to significantly skew the interpretation of crater counts on very young surfaces, such as the ejecta blankets of recent craters. Figure 8 shows the extent to

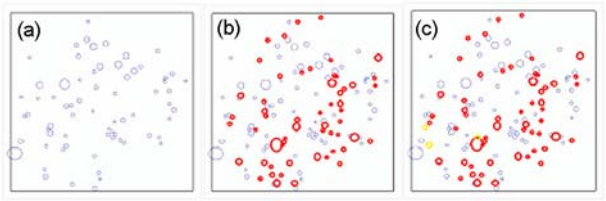

Figure 9. The superposition relationships determined for the Newton-A region using the common age of the Tycho secondary craters. (a) The region before the Tycho event, about 100 Myr. (b) The region just following the emplacement of the Tycho secondaries, shown in red atop the preexisting craters in blue. (c) The region today, with the primaries formed since the Tycho event in yellow.

which similar, undetected secondary populations could contaminate hypothetical lunar terrains of various ages. These plots were created by adding a density representative of the secondary crater populations at Newton and Newton-A ($c = 3.76 \times 10^{-3}$) to the densities predicted by *Neukum et al.* [2001] for 10 Myr, 100 Myr, 1 Gyr, and 4 Gyr lunar terrains. For purposes of discussion, we assume that the secondary densities measured at Newton and Newton-A are typical of hidden ray populations and that current lunar isochrons are based on primary-dominated counts at small diameters (in other words, that the secondary populations measured here occur in isolated regions). We also ignore the probable erasure of some underlying primary craters that would occur during emplacement of the hypothetical secondary layer. With these assumptions, the result of failing to remove hidden ray secondary craters from counts in regions where they exist can be summarized as follows:

[20] 1. Surfaces with true ages older than about 3.4 Gyr will be largely unaffected by the addition of the hidden ray population. The erroneous increase in age will be on the order of few percentages, as at Newton and Newton-A. For small terrain units where the $D < 1$ km population is important for age dating, this is on the order of, or less than, the uncertainty in age introduced by counting statistics.

[21] 2. Surfaces with true ages around 3.4 Gyr superposed by hidden ray secondary craters will contain roughly equal numbers of 1 km diameter primary and secondary craters. For small terrain units where the $D < 1$ km population is important for age dating, the increase in age by improperly including the secondary craters is slightly less than 20%, from 3.4 to around 4 Gyr.

[22] 3. Surfaces with ages of less than 3.4 Gyr will be dominated by secondary craters at diameters below 1 km if "hidden ray" craters are present. The result of improper inclusion of hidden ray secondary craters in counts for age dating on a surface with a true age of 1 Gyr, for example, would be to make the surface appear 3.48 Gyr old, about 2.5 times older. Again, this is primarily relevant for small terrain units where the $D < 1$ km population is important for age dating. Young crater ejecta blankets and some volcanic features on the Moon fall within these age and size bounds. Because of the potential to significantly alter the inferred ages of such features, it will be vital to quantify how common such hidden rays are on the lunar surface.

5.2. Post Tycho Primary Impacts

[23] Identification of secondary craters by the presence of asymmetric ejecta blankets also provides a convenient benchmark around which the local superposition relationships can be investigated. The Tycho secondaries in question have a well constrained age of ~96 Myr derived from Tycho ray material gathered by Apollo astronauts [*Arvidson et al.*, 1976]. Using the known age of the secondary layer, three "snapshots" in time of the Newton and Newton-A floors were produced: one prior to the Tycho event, one of the regions just after Tycho was emplaced around 96 Myr, and one of the present crater floor with the layers labeled in time (Figure 9). Primary craters were determined to be older than the Tycho secondaries based on three criteria: lack of a high-CPR ejecta blanket, obvious rim erosion and floor flattening relative to the fresher secondary layer, or superposition of a high-CPR ejecta tail. Conversely, primaries younger than the inferred Tycho secondary features were identified based on sharp rim morphology coincident with symmetric high-CPR ejecta blankets. The rim erosion of the primary craters (and subsequent infill leading to shallow floors) older than the secondary crater layer may be the result of "sand blasting" of the region by secondary and tertiary ejecta, which is why it is indicative of craters that were already on the surface when the secondary layer was emplaced. Given a larger survey, this method could provide a strong constraint on the production function of small lunar primaries during the last 100 Myr.

6. Summary

[24] CPR maps of Newton and Newton-A craters reveal a cluster of small ($D < 2$ km) craters with highly asymmetric ejecta blankets, aligned roughly parallel to one another and along the same direction as an optical Tycho ray several hundred kilometers to the northwest. We interpret these CPR bright ejecta blankets as secondary ejecta belonging to small Tycho secondary craters. Best fit power law slopes ($b = -2.20 \pm 0.27$ and $b = -2.30 \pm 0.22$) for the secondary populations at Newton and Newton-A are shallower than the canonical $b = -3$ or -4 for secondary craters. However, secondary crater size frequency distributions display a downturn at small diameters that is not typically included in the calculation of the power law slope. The secondary SFDs at Newton and Newton-A represent this smaller diameter population and are in agreement with the behavior measured at small diameters by other workers [*Hirata and Nakamura*, 2006; *Dundas and McEwen*, 2007]. The high number density of secondary craters measured ($c \sim 10^{-3}$ craters/km^2) and the orientation of their ejecta along the Tycho radial direction suggest that this population is a "hidden" extension of the visible Tycho ray that superposes Clavius crater. As other lunar rays may continue as secondary crater over densities beyond where they are visible as high-albedo features, the degree of possible contamination by similar populations on lunar terrains over a range of ages was explored. The extent of contamination was quantified by adding the average secondary crater density at Newton and Newton-A (as a function of crater diameter) to the densities predicted by *Neukum et al.* [2001] for 10 Myr, 100 Myr, 1 Gyr, and 4 Gyr lunar terrains. The resulting ages of the combined populations were compared to the "uncontaminated" ages represented by

the *Neukum et al.* [2001] isochrons. In the presence of a "hidden ray," primary and secondary craters can be expected to occur in roughly equal numbers on lunar terrains with primary crater densities corresponding to 3.4 Gyr. For hidden rays superposing surfaces with primary crater densities corresponding to ages younger than 3.4 Gyr, secondary craters would dominate all counts below 1 km. Because of the potential to significantly alter the inferred ages of young features, future work should investigate where and how commonly such hidden rays occur on the lunar surface.

References

Arvidson, R., et al. (1976), Cosmic ray exposure ages of Apollo 17 samples and the age of Tycho, *Proc. Lunar Planet. Sci. Conf. 7th*, 2817–2832.

Bierhaus, E. B., et al. (2001), Pwyll secondaries and other small craters on Europa, *Icarus*, *153*, 264–276.

Bierhaus, E. B., C. R. Chapman, and W. J. Merline (2005), Secondary craters on Europa and implications for cratered surfaces, *Nature*, *437*, 1125–1127.

Campbell, B. A., and D. B. Campbell (2006), Regolith properties in the south polar region of the Moon from 70 cm radar polarimetry, *Icarus*, *180*, 1–7.

Campbell, D. B., et al. (2006), No evidence for thick deposits of ice at the lunar south pole, *Nature*, *443*, 835–837.

Crater Analysis Techniques Working Group (1979), Standard techniques for presentation and analysis of crater size frequency data, *Icarus*, *37*, 467–474.

Dundas, C. M., and A. S. McEwen (2007), Rays and secondary craters of Tycho, *Icarus*, *186*, 31–40.

Hawke, B. R., et al. (2004), The origin of lunar crater rays, *Icarus*, *170*, 1–16.

Hirata, N., and A. Nakamura (2006), Secondary craters of Tycho: Size-frequency distributions and estimated fragment size-velocity relationships, *J. Geophys. Res.*, *111*, E03005, doi:10.1029/2005JE002484.

Hurst, M., M. P. Golombek, and R. Kirk (2004), Small crater morphology within Gusev crater and Isidis Planitia: Evidence for widespread secondaries on Mars, *Lunar Planet. Sci.*, *XXXV*, Abstract 2068.

McEwen, A. S., et al. (2005), The rayed crater Zunil and interpretations of small impact craters on Mars, *Icarus*, *176*, 351–381.

Neukum, G. (1983), Meteoritenbombardement und Datierung planetarer Oberflachen. Habilitation dissertation for faculty membership, Ludwig Maximillians, University of Munich, Munich, Germany, 186 pp.

Neukum, G., and B. A. Ivanov (1994), Crater size distributions and impact probabilities on Earth from lunar, terrestrial planet, and asteroid cratering data, in *Hazards Due to Comets and Asteroids*, edited by T. Gehrels, pp. 359–416, Univ. Arizona Press, Tucson, Ariz.

Neukum, G., and D. Wise (1976), Mars: A standard crater curve and possible new time scale, *Science*, *194*, 1381–1387.

Neukum, G., B. A. Ivanov, and W. K. Hartmann (2001), Cratering records in the inner solar system in relation to the lunar reference system, *Space Sci. Rev.*, *96*, 55–86.

Oberbeck, V. R., and R. H. Morrison (1973), On the formation of lunar herringbone pattern, *Proc. Fourth Lunar Sci. Conf.*, *Geochim. Cosmochim. Acta*, *1*, 107–123, Pergamon.

Pike, R. J., and D. E. Wilhelms (1978), Secondary-impact craters on the Moon: Topographic form and geologic process, in *Proc. Lunar Planet. Sci. Conf. 9th*, p. 907–909, Lunar and Planetary Institute, Houston, Tex.

Preblich, B. (2005), Mapping Rays and Secondary Craters from Zunil, Mars, Thesis, University of Arizona, Tucson, Ariz., 77 pp.

Shoemaker, E. M. (1965), Preliminary analysis of fine structure of the lunar surface in Mare Cognitum, in *The Nature of the Lunar Surface*, edited by Hess et al., pp. 23–77, Johns Hopkins Univ. Press, Baltimore, Md.

Werner, S. C., B. A. Ivanov, and G. Neukum (2009), Theoretical analysis of secondary cratering on Mars and an image-based study on the Cerberus Plains, *Icarus*, *200*, 406–417.

Wilhelms, D. E., V. R. Oberbeck, and H. R. Aggarwal (1978), Size-frequency distributions of primary and secondary impact craters, *Proc. Lunar Planet Sci. Conf.*, *9th*, 3735–3762.

Wilhelms, D. E., et al. (1979), Relative ages of lunar basins, *Reports of Planetary Geology Program*, *1978–1979*, 135–137.

B. A. Campbell and L. M. Carter, Center for Earth and Planetary Studies, National Air and Space Museum, Smithsonian Institution, Washington, DC 20560, USA.

D. B. Campbell and K. S. Wells, Astronomy and Space Sciences Department, Cornell University, 514 Space Sciences Building, Ithaca, NY 14853, USA. (kassiew@astro.cornell.edu)